Experimental Investigation of a Circulating Fluidized-Bed Reactor to Capture CO_2 with CaO

N. Rodríguez, M. Alonso, and J. C. Abanades
Spanish Research Council, INCAR-CSIC, C/Francisco Pintado Fe, 26, 33011 Oviedo, Spain

DOI 10.1002/aic.12337
Published online July 30, 2010 in Wiley Online Library (wileyonlinelibrary.com).

Calcium looping processes for capturing CO_2 from large emissions sources are based on the use of CaO particles as sorbent in circulating fluidized-bed (CFB) reactors. A continuous flow of CaO from an oxyfired calciner is fed into the carbonator and a certain inventory of active CaO is expected to capture the CO_2 in the flue gas. The circulation rate and the inventory of CaO determine the CO_2 capture efficiency. Other parameters such as the average carrying capacity of the CaO circulating particles, the temperature, and the gas velocity must be taken into account. To investigate the effect of these variables on CO_2 capture efficiency, we used a 6.5 m height CFB carbonator connected to a twin CFB calciner. Many stationary operating states were achieved using different operating conditions. The trends of CO_2 capture efficiency measured are compared with those from a simple reactor model. This information may contribute to the future scaling up of the technology. © 2010 American Institute of Chemical Engineers *AIChE J,* 57: 1356–1366, 2011

Keywords: CO_2 capture, calcium looping, capture efficiency, carbonation, calcination

Introduction

According to the intergovernmental panel on climate change (IPCC), CO_2 capture and storage "would be an option in the portfolio of actions for stabilization of greenhouse gas concentrations as allowing for the continued use of fossil fuels."[1] Large-scale CO_2 capture technology already exists in the gas, oil, and chemical industries, where CO_2 and other key gases (H_2 or O_2) in CO_2 capture systems are routinely separated from different process streams. Theoretically, these technologies could be adapted for the capture of CO_2 in flue gases from fossil fuel power plants. However, if existing technologies are provided with the necessary incentives, it is widely accepted that there is further scope for large reductions in CO_2-capture costs and energy efficiency penalties by means of a second wave of CO_2 capture technologies.

A promising method of capturing CO_2 from power plant flue gases is to use a lime carbonation–calcination cycle (or "calcium looping") such as that illustrated in Figure 1. This process was originally proposed by Shimizu et al.[2] for postcombustion applications. However, the earliest research on CaO as a regenerable sorbent goes back more than a century (see recent reviews of Harrison[3] and Anthony[4]). As early as 1967, Curran et al.[5] reported key experimental results in a pilot plant developed for the "acceptor" process, involving two interconnected fluidized-bed reactors (gasifier-acceptor and combustor-calciner) operating at very high pressure and temperatures. In recent years, interest in this research area has grown dramatically. The pioneering works of Harrison and coworkers[6–8] on precombustion routes have been cited more than 200 times and a similar trend can be observed for the early works on postcombustion.[2,9,10] The IEA greenhouse gas program recently launched a new research network on high-temperature solid looping cycles.[11] Research work on calcium looping attracted a strong worldwide R&D response at the first network meeting in Oviedo (Spain), with some electricity companies and manufacturing companies announcing plans for the rapid development of postcombustion technology[11] over the next decade.

The increasing interest in Ca-looping process for postcombustion applications can be attributed to the advantages they

Correspondence concerning this article should be addressed to N. Rodríguez at nuria@incar.csic.es.

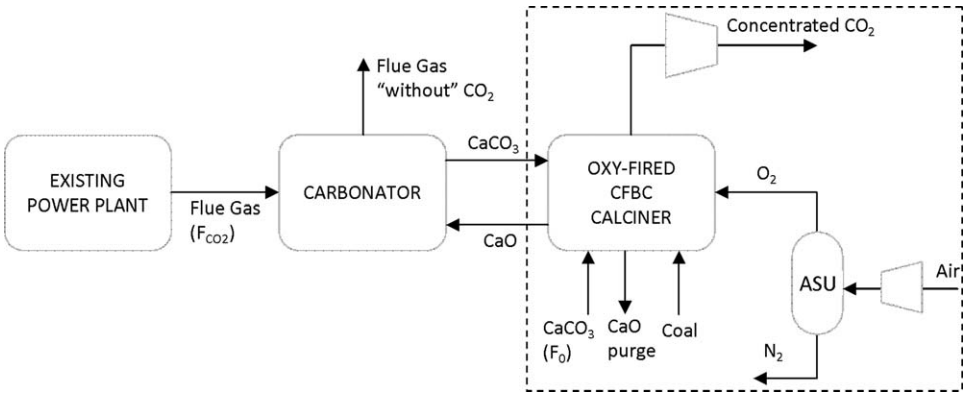

Figure 1. Schematic of a calcium looping system for capturing CO_2 from an existing power plant.

The oxyfired circulating fluidized-bed combustor acts as calciner and generates more power.

offer[2,4]: CO_2 is captured at high temperatures from the combustion flue gas of a power plant in a carbonator operating between 600°C and 700°C. Therefore, the energy required to calcine $CaCO_3$ in the regeneration step can be recovered at the high temperatures of the exothermic carbonator. As can be seen in Figure 1, when the solids leave the carbonator (with CaO partially converted to $CaCO_3$), they are directed to a second fluidized bed where calcination/regeneration takes place. Coal in the calciner burns in an atmosphere of O_2/CO_2 at temperatures above 900°C, thus producing the heat necessary to calcine the $CaCO_3$ back into CaO and CO_2. The calciner operates with oxygen supplied by an air separation unit, but other sources of heat for calcination may be used in the future.[12] The CO_2 captured from the flue gases as $CaCO_3$ and the CO_2 produced by the oxyfired combustion of coal in the calciner are recovered in concentrated form from the calciner gas. After the CO_2 has been purified and compressed, it is transported and stored in deep geological formations. The calciner requires energy to heat the incoming gas and solid streams up to the calciner temperatures and to provide the heat necessary for the endothermic calcination of $CaCO_3$. A considerable fraction (35–55%) of the total energy entering the system is used[13] in the calciner. Most of this energy leaves the system in mass streams at high temperature (at $T > 900$°C) or is recovered as carbonation heat in the carbonator (at around 650°C). Thus, the large energy input into the calciner comes out of the system as high-quality heat that can be used in a highly efficient steam cycle.[2,12,14] Thus, the calciner acts like a new oxyfired fluidized-bed power plant. However, in this new power plant, the CO_2 output can be almost double thanks to the CO_2 captured in the carbonator as $CaCO_3$, which is then converted back to CaO and CO_2 in the oxyfired calciner.

The carbonator reactor depicted on the left-hand side of Figure 1 is a key process unit that is designed and operated in such a way as to achieve high-capture efficiencies of CO_2 from the flue gas. The flow rates of flue gases from an average 1000-MW-power plant are about 300 $Nm^3\ s^{-1}$. Bringing this huge flow of gas into contact with CaO particles is only possible in reactors with a very high gas throughput per unit of area such as circulating fluidized-bed (CFB) reactors. In addition, when using CFB technology for the carbonator, we can take advantage of their mechanical similarities to large scale circulating fluidized-bed combustors that operate with gas velocities, solids circulation rates, and types of solid materials that are very similar to those required for the carbonation–calcination loop. Moreover, CFB are now available as supercritical power plants,[15] which makes this technology even more interesting for Ca looping.

Despite the increasing number of published works that deal with different aspects of calcium looping systems (sorbent performance and reactivation studies, batch experiments and modeling, process simulation work, etc), recently reviewed in Anthony,[4] there is an obvious lack of experimental information on the performance of fluidized-bed carbonator reactors at atmospheric pressure. What is more, this shortcoming is in sharp contrast with the recent rapid progress achieved in the precombustion route. Koppatz et al.[16] have reported results on hydrogen production by means of steam gasification in the presence of CaO in an 8-MW-biomass input test facility operating at atmospheric pressure with interconnected CFBs. There is no similar work on Ca-based postcombustion applications and the work that is being carried out is on a much smaller scale. An earlier set of experimental results obtained in a batch fluidized bed of CaO at the CANMET CFB combustor pilot plant[17] proved that CO_2 could be captured from flue gases with CaO at atmospheric pressure in a batch fluidized bed of CaO using reasonable gas residence times and bed inventories. The recently published results of other batch tests carried out at laboratory scale confirm the deactivation trends of sorbent and basic bubbling reactor modeling tools.[18,19] Lu et al.[20] achieved stable conditions in a bubbling fluidized-bed carbonator interconnected with a CFB calciner in fully continuous mode. This group[21] also reported that the operation of an oxyfired calciner is not very different from the operation of CFB combustors operating at similar high temperatures (over 900°C), although a further deterioration of the sorbent was observed during oxyfired calcination. Charitos et al.[22] also reported on the operation experience of a 10-kW-dual fluidized bed (a bubbling carbonator connected to a CFB calciner) in which they achieved precise control of the sorbent circulation rate between reactors by means of a high-temperature cone valve. Recently, Alonso et al.[23] reported the results of first continuous and stable test in a CFB carbonator coupled to a CFB calciner. CO_2 capture efficiencies in the carbonator reactor ranged between 70% and 97% under realistic flue gas conditions. However, there is a very limited amount of

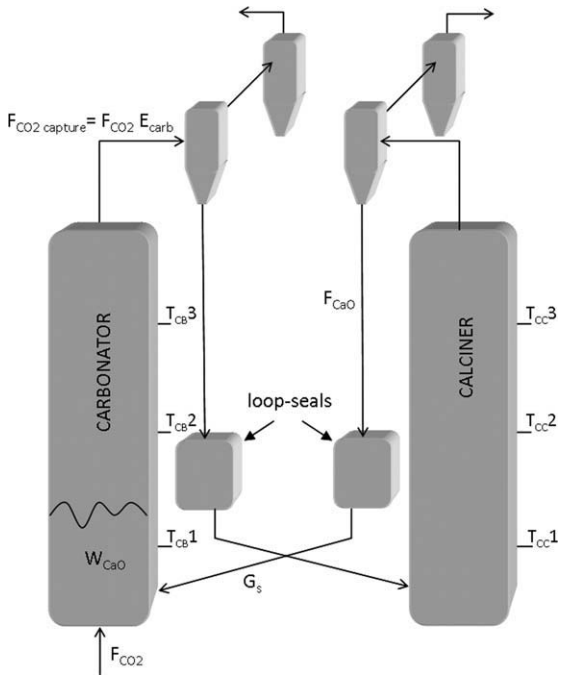

Figure 2. Schematic of the 30-kW test facility at INCAR-CSIC.

experimental information available to allow the prediction and analysis of the key trends in reactor performance as a function of the operating conditions.

The purpose of this work is to investigate the effects of the key variables on CO_2 capture efficiency in a CEB carbonator that is continuously fed with CaO generated by an interconnected fluidized-bed calciner. A simple reactor model is used to interpret the observed trends as a function of the sorbent properties and operating variables, so that more detailed insights can be gained as to how to design and operate these new reactors when they are used at a larger scale.

Experimental

Figure 2 shows a scheme of the 30-kW test facility designed and built at INCAR-CSIC. It is made up of two interconnected CEB reactors: a carbonator and an air-fired calciner. The carbonator is 6.5 m and the calciner 6.0 m in height. Both the reactors have an internal diameter of 0.1 m. The loop-seals and risers up to a height of 2.5 m are surrounded by electric ovens. The ovens are independently controlled heating elements that can be switched off in the carbonator after start up to release the excess heat generated during the carbonation reaction.

A mixture of simulated flue gas (air from a blower and carbon dioxide from a Dewar) is fed into the carbonator. The carbon dioxide reacts with active calcium oxide coming from the calciner into the carbonator at temperatures between 600°C and 700°C. The calcium carbonate formed in the carbonator is regenerated under typical combustion conditions in the CFB calciner (in the experimental conditions of this work: air-fired combustion at 800–900°C with a 2–6% air excess).

A mixture of gases and solids leaves the risers through the primary cyclones. The solids then fall out of the cyclones down vertical standpipes to the bubbling fluidized-bed loop seals. As the loop-seals are continuously aerated with air, the solids flow over them toward inclined standpipes that direct them to the opposite reactor.

Continuous gas analyses (carbon dioxide, oxygen, and carbon monoxide) can be carried out from different points in the installation, but mainly after the secondary cyclones, where the gas has low-solids content. The risers are also fitted with zirconia oxygen probes so that local O_2 content can be measured, adding confidence to the O_2 composition measurements made by the gas analyzer. This is particularly important in a small test facility such as ours, because air in the loop seal may amount to 20% of the total gas inflow the risers and it is uncertain where this aeration gas will go. In normal circulation conditions, it should follow the circulating solids down the inclined standpipe into the riser. Thus, the oxygen probe should give the same reading for average oxygen content as the gas analyzer. However, under low-solids circulation rates, a fraction of the air fed into the loop seal travels upward toward the cyclone. In this case, the oxygen content measured by the zirconia probe at the exit of the riser is smaller than that measured by the gas analyzer after the secondary cyclone. In some cases, this air leakage from the loop seal also affects the solids capture efficiency in the primary cyclone, resulting in a rapid loss of mass inventory in the primary circulation loop. Therefore, when a mismatch in O_2 concentration is detected between the zirconia probes and analyzer, measures must be taken (the reduction of aeration in the loop seal and/or the introduction of more solids into the primary circulation loop) to re-establish a high-solids circulation.

All the electric signals from the thermocouples, pressure transducers, gas analyzers, and mass flow controllers are collected on a computer. Furthermore, there is a solids bypass just below the loop seals where solids can be extracted and their circulation rates (G_s, kg m^{-2} s^{-1}) can be measured. This is done by diverting the solids to a dead volume for a certain period of time. These solids are then subjected to analysis together with other solid samples that are extracted directly from the riser ports. Quartz windows located in the inclined standpipes between the loop-seals and the risers are used to visually confirm that the solids circulation rate is stable during the experiment and/or for specific time intervals between individual measurements. All the solids samples are analyzed to determine their total calcium oxide content and the amount of calcium that has been converted to calcium carbonate. Selected samples are taken from the carbonator to measure the carbonation reaction rate in a thermobalance specially designed for multicycle experiments.[24] Two kind of high-purity limestones (>98% calcium carbonate) were used in the experiments. The limestones had an original particle size range of <350 μm and an average particle size of around 90 μm after attrition of the material, but most of the size degradation takes place after the first calcination.[25] Fresh batches of limestone were occasionally added to the system to maintain the level of solids inventories and the circulation rates.

In a characteristic run, a batch of 20 kg of limestone, or solids from a previous run, is loaded into the loop-seals and

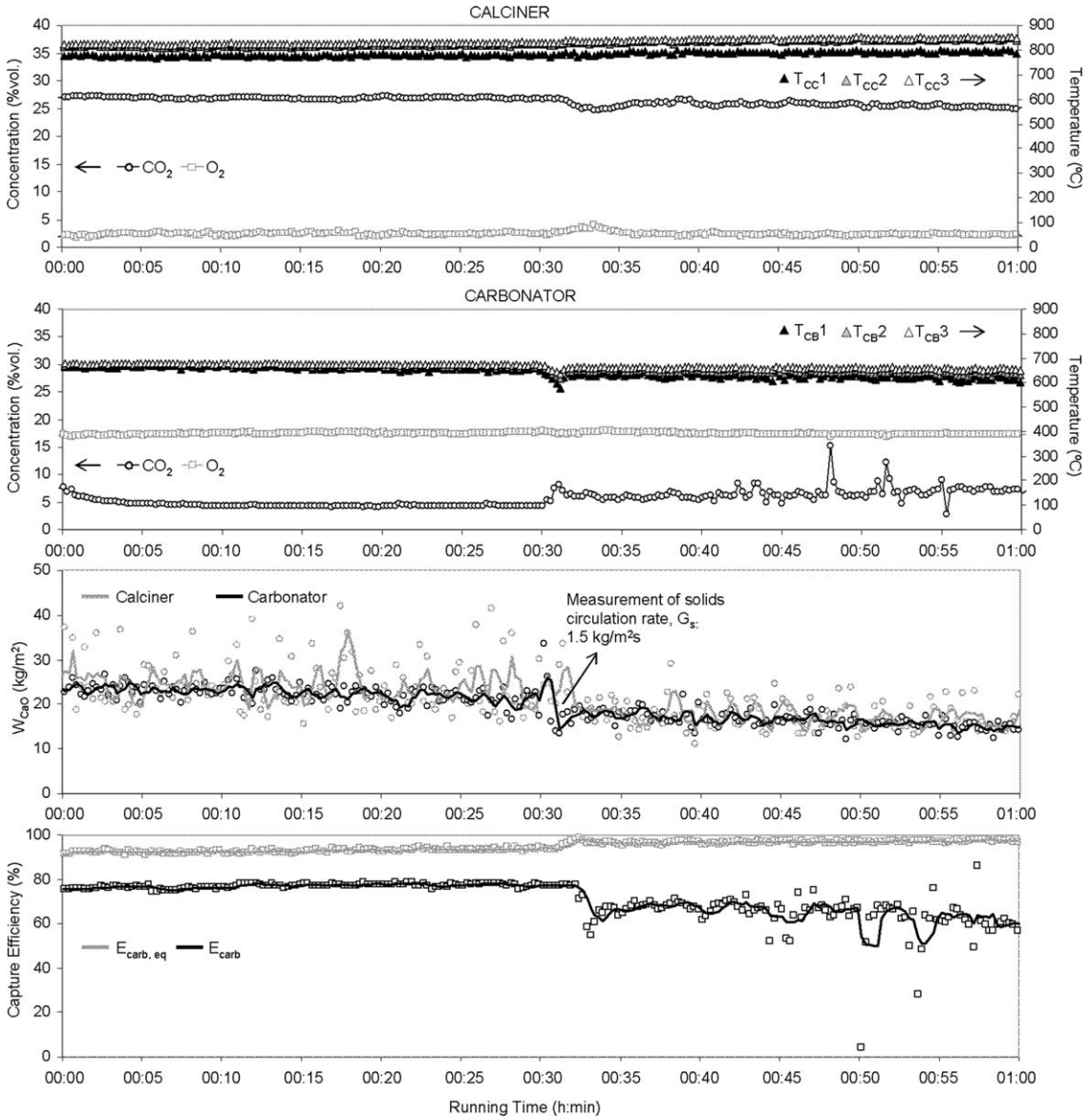

Figure 3. Results of an experiment carried out in the interconnected circulating fluidized-bed facility of Figure 2.

$T_{CC}1$, $T_{CC}2$, $T_{CC}3$: measurements of temperature in the calciner; $T_{CB}1$, $T_{CB}2$, $T_{CB}3$: measurements of temperature in the carbonator; E_{carb}, $E_{carb,\ eq}$: CO_2-capture efficiency and maximum CO_2-capture efficiency limited by the equilibrium, respectively.

the risers. Almost complete calcination is achieved by burning coal in both the carbonator and the calciner, with all the ovens switched on. Temperatures during calcination are around 800°C in both risers but rapid temperature increases to well over 1000°C may take place if the circulation or calcination of solids is accidentally interrupted by a lack of $CaCO_3$. After calcination is completed, the coal feed, the ovens in the carbonator, and the oven in the loop-seal that feeds solids to the carbonator are switched off. From this point, the temperature falls and the CO_2 feed to the air blown carbonator is switched on. After a certain period of adjustment, stationary conditions are re-established in terms of temperature and solids circulation, as can be seen in Figure 3. This figure shows a typical plot corresponding to an experimental period of 1 h. In the 2 first graphs, the CO_2 and O_2 compositions in the calciner and in the carbonator (left axis) are presented together with the temperatures (right axis) at three different heights along the risers. The third graph shows the state of the bed inventory in each riser (calculated assuming that the ΔP measured in the riser is due to the bed inventory (W_{CaO}) as in minimum fluidization conditions ($\Delta P = W/A$)). In the last graph, the gas composition in the carbonator has been plotted on the basis of instant capture efficiency calculated as a function of the experimental concentration of CO_2 at the exit of the carbonator. This instant capture efficiency is compared with the maximum efficiency allowed by the equilibrium at the average temperature in the carbonator reactor at that particular time.

The temperature in the calciner reactor is between 800°C and 850°C, whereas in the carbonator reactor it is between 630°C and 700°C. The conditions in the calciner should be considered in the light of the high-CO_2 concentration and

Table 1. Range of Operating Conditions and Range of Main Parameters Involved in the Experimental Work

Range of Main Parameters in the Carbonator		
Temperature (°C)	T_{carb}	568–722
Superficial gas velocity (m s^{-1})	u	1.1–3.3
Inlet CO_2 volume fraction	$v_{CO_2,0}$	0.03–0.25
Solids bed inventory (kg m^{-2})	W_{CaO}	33–357
Maximum average conversion	X_{ave}	0.08–0.41
Fraction of active CaO	X_{active}	0.01–0.19
Net carbonation conversion	ΔX	0.01–0.13
Capture efficiency	E_{carb}	0.30–0.92

low-oxygen concentration at the outlet of the calciner. The CO_2 released in the calciner is around 27%. A combustion mass balance shows that around 16% is due to combustion with the air of the coal feed. Therefore, at this point, the calciner flue gas contains an additional 11% of CO_2, which translates into the release of about 4 mol m^{-2} s^{-1} of CO_2 due to the calcination of the $CaCO_3$ transported by the circulating solids. By contrast, at the outlet of the carbonator, the CO_2 concentration is around 7% during most of the experiment, whereas the CO_2 concentration at the entrance to the carbonator is about 20 vol % of CO_2. By adjusting with the O_2 probe, it was found that a small amount of CO_2 was generated in the carbonator by the unburned coal from the calciner. In these conditions, the capture rate in the carbonator was then ~4 mol m^{-2} s^{-1}, virtually identical to the average rate of CO_2 released in the calciner in the same experimental period. As can be seen from the figure, capture efficiency is stable above 70% (with superficial gas velocities of around 3 m s^{-1}). A lower value is only obtained when solids are extracted from the system to measure the solids circulation rate (after around 30 min according to graphs). During this measurement period, the flow of solids to the carbonator momentarily ceases and the solids inventory in the carbonator decreases causing a drop in CO_2 capture efficiency until new solids are fed into the carbonator.

Each completed experimental period is characterized by a given set of operating conditions and is subjected to continuous measurements of the gas compositions from both reactors (see Figure 3) and by an analysis of the solid samples extracted from different ports (in the carbonator, the calciner, and just below the loop seal that introduces solids into the carbonator). Therefore, for each set of operating conditions, there is an experimental average carbonator temperature (T_{carb}), an average calcination temperature (T_{calc}), the state of the solids inventory in the risers (W_{CaO}, from the readings of the ΔP in the riser), the CO_2 concentration at the carbonator inlet ($v_{CO_2,0}$), the carbonate content of the solids leaving the carbonator and the calciner (X_{carb}, X_{calc}), and the net carbonation conversion ($\Delta X = X_{carb} - X_{calc}$), which is the difference in the $CaCO_3$ composition of the solid samples extracted before and after the carbonator reactor. The difference indicates the carbon dioxide that has reacted with CaO in the bed. It is also important, as will be seen below, to measure X_{ave}, which is the maximum carbonation achieved by the solids samples at the end of the fast carbonation period in a standard thermo gravimetric (TG) carbonation test.[24,26] X_{ave} gives the maximum CO_2 capture capacity of the solids extracted from the bed for estimating at any one point the fraction of active CaO in the bed ($X_{active} = X_{ave} - X_{carb}$).

This installation has been in operation for around 450 h, around 30% of this time corresponding to relatively stationary periods of carbonation and calcinations like the one presented in Figure 3. The range of operating conditions and the main parameters involved in the carbonation reaction are presented in Table 1. The experiments were carried out using two different limestones that presented very similar behaviors to other high-purity limestones, and one main type of coal of low sulfur and ash content (67.89% C, 4.97% H, 0.2% S, 19.91% H_2O, 0.92% N, and 3.78% ash). Some of the later experiments were conducted using a different coal in the calciner with ash and sulfur contents of 19.02% and 0.72%, respectively. Although sulfur reacts with CaO at the temperature of the calciner reactor, which should cause a decrease in the global capture efficiency, the initial batch of solids fed into the system is too large (20 kg) for our test rig to handle (because of the large volume of the loop seals). Therefore, it would take well over 700 h to convert the Ca initially loaded into the system to $CaSO_4$. For this reason, no suitable results from this rig can be reported at present regarding the role of sulfur. The effects of SO_2 on CaO looping systems have been investigated at particle level in more detail in other works.[27–29]

Discussion

The main objective of this section is to analyze and discuss the CO_2 capture efficiency achieved in the carbonator as a function of the experimental conditions. Flue gas entering the carbonator reactor contains CO_2 (F_{CO_2} in mol m^{-2} s^{-1}), which will react with the active CaO present in the riser bed inventory. Capture efficiency in the carbonator can therefore be expressed as:

$$E_{carb} = \frac{\text{CO}_2 \text{ reacting with CaO in the bed}}{\text{CO}_2 \text{ entering the bed in the flue gas}} \quad (1)$$

Moreover, new calcined particles are continuously arriving in the carbonator and are converted to $CaCO_3$. Thus, the overall mass balance in the system can be expressed as:

$$\begin{pmatrix} \text{CO}_2 \text{ reacting with} \\ \text{CaO in the bed} \end{pmatrix} = \begin{pmatrix} \text{CaCO}_3 \text{ formed in the} \\ \text{circulating stream of CaO} \end{pmatrix} = \begin{pmatrix} \text{CO}_2 \text{ removed from} \\ \text{the gas phase} \end{pmatrix} \quad (2)$$

The central term of the balance means that the $CaCO_3$ formed in the circulating stream through the reactor must be equal to the CO_2 removed from the gas phase. In the stationary state period, when the solid circulation rates and the carbonation conversions abandoning the reactor have not changed with time during the period:

$$F_{CaO}(X_{carb} - X_{calc}) = F_{CO_2} E_{carb} \quad (3)$$

where F_{CaO} is the CaO circulation rate in mol m^{-2} s^{-1}, X_{carb} is the average carbonation conversion of the solids achieved in the carbonator reactor, and X_{calc} is the carbonate content of the solids coming from the calciner (X_{calc} should be zero or close to zero if the calciner reactor is working correctly). Figure 4 shows a comparison of the experimental terms in Eq. 3 for

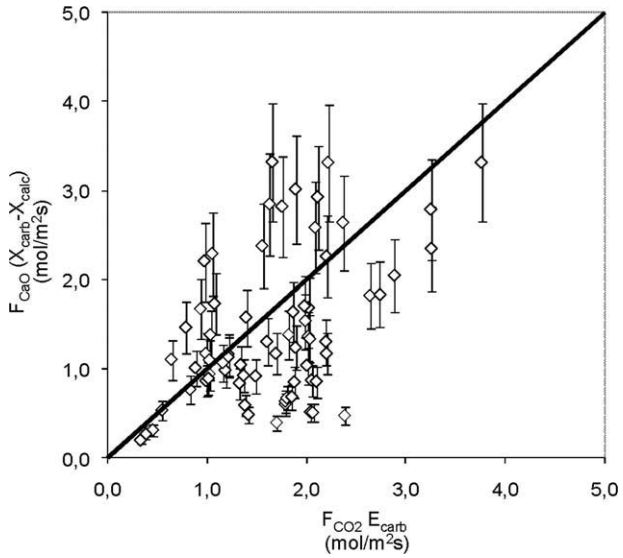

Figure 4. Experimental comparison between the CO_2 removed in the carbonator from the gas phase and the $CaCO_3$ carried in the solid circulating stream between carbonator and calciner.

many experimental periods like the one finishing at 00:33 in Figure 3 with an extraction of solids to measure circulation rates. The plot in Figure 4 compares the CO_2 that has disappeared from the gas phase in the carbonator (from flow gas measurements and gas analysis) and the $CaCO_3$ formed in the circulating stream. The closure of the mass balance represented in Figure 4 and Eq. 3 shows a wide scatter of the experimental points due to high-experimental uncertainties in the estimation of solid circulation rates and in the determination of the average carbonation conversion (each dot in the graph has a $\pm 20\%$ error bar to account for them). This is because the average solids circulation rate is a parameter difficult to measure in any experimental CFB system. Also, the small solids samples taken sporadically from a solid port of the reactors are not representative enough of the bed inventory and, therefore, have, inevitably, a substantial uncertainty in the actual carbonate conversion. Finally, in dynamic tests (not included in the figure), the mass balance represented by Eq. 3 is not achieved because the conversion of the solids in the bed is continuously changing with time due to the lack of sufficient circulating solids or due to the sudden addition of a batch of fresh CaO to the carbonator (Alonso et al.,[23]).

In stationary state periods, Eq. 2 allows the formulation of a CO_2 mass balance that is more suitable for data interpretation and reactor design:

$$F_{CO_2} E_{carb} = \frac{W_{CaO}}{PM_{CaO}} \frac{dX_{carb}}{dt}\bigg|_{reactor} \quad (4)$$

where W_{CaO} is the total inventory of solids in the carbonator (kg m^{-2}), PM_{CaO} is the average molar weight of the solids inventory in the carbonator (kg mol^{-1}), and $dX_{carb}/dt|_{reactor}$ is the average reaction rate of the solids in the reactor (s^{-1}) at the average temperature and average CO_2 concentration in the carbonator. As there are no other solids in the system than CaO or $CaCO_3$, the bed inventory of solids can be estimated from the pressure drop measurements in the reactors and the carbonate content measured during the analysis of solids samples. This direct measurement of the bed inventory in the reactor avoids the need for a hydrodynamic model to estimate this critical parameter in this particular experimental setup. Future models of the reactor aimed at scaling up will have to incorporate such a hydrodynamic submodel to estimate this inventory as a function of operating conditions, solid characteristics, and bed geometry.

To estimate the reaction rate term of Eq. 4, on the basis of the previous analysis carried out for modeling the carbonation process of a batch of CaO,[17] we assume that the bed contains three types of sorbent particles: a fraction of active CaO reacting in fast regime (X_{active}), a fraction of inactive CaO from previous carbonation–calcination cycles, and a fraction of $CaCO_3$ resulting from the carbonation conversion (X_{carb}). In these conditions, the reaction rate can be estimated from independent kinetic data provided that the fraction of active CaO in the bed inventory of solids and the average concentration of CO_2 in the gas phase are known. Assuming a first-order carbonation reaction rate, we obtain the following expression:

$$\frac{dX}{dt}\bigg|_{reactor} = \varphi_e \, k_{reac-max} \, X_{active} \left(\upsilon_{CO_2} - \upsilon_{CO_2,eq}\right)_{reactor} \quad (5)$$

where $k_{reac\text{-}max}$ is the reaction rate constant of active CaO, X_{active} is the active fraction of the CaO in the carbonator reactor, and v_{CO_2} and $v_{CO_2,eq}$ are the average volume fraction and the equilibrium volume fraction of CO_2 in the reactor, respectively. The rate constant $k_{reac\text{-}max}$ was estimated to be around 0.37 s^{-1} for the two limestones used in this work, which is consistent with the results of independent thermobalance experiments reported elsewhere[26] and also with

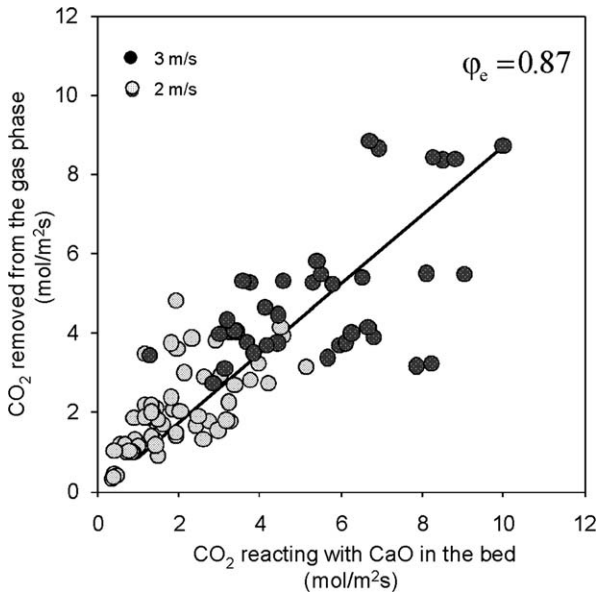

Figure 5. Comparison of the molar flow of CO_2 removed from gas phase with the CO_2 molar flow reacting with CaO in the bed of the carbonator reactor.

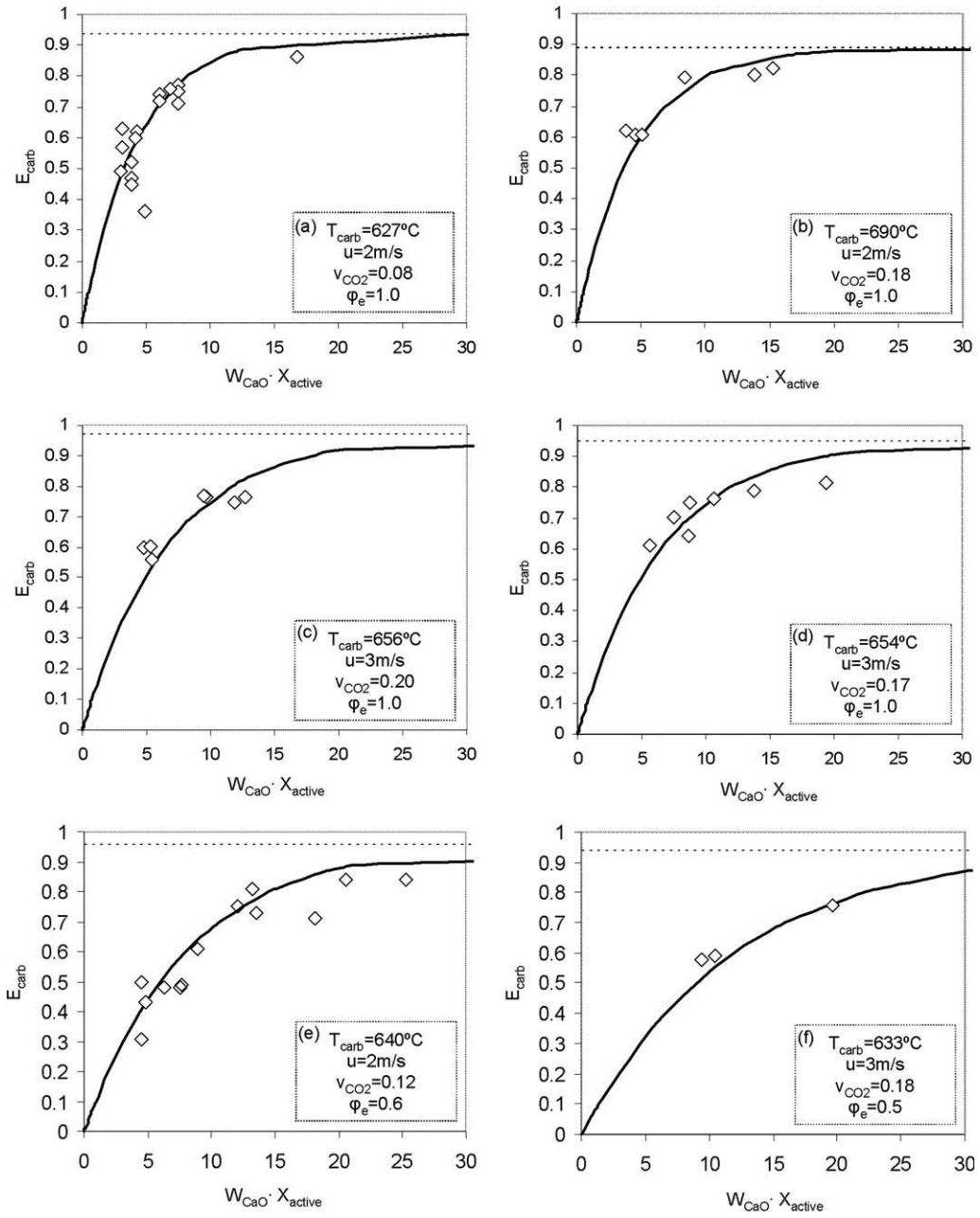

Figure 6. Capture efficiency as a function of the active inventory of solids in the carbonator for selected data sets obtained under the same operating conditions (average operating conditions in the experiments used to calculate the model line).

previous publications reporting little or negligible effect of temperature on the rates of carbonation in the interval of temperatures of interest for this work.[30,31] Grasa et al.[32] recently applied the pore model of Bhatia and Perlmutter[30] to multiple carbonation calcination cycles, obtaining a good quality fit for the full range of reactivities shown by the CaO particles in these systems. Moreover, for most of the experiments reported here, which are characterized by modest values of X_{ave} (highly cycled particles), the simple equation represented in Eq. 5 yields sufficiently accurate rates of reaction. The volume fraction of CO_2 in the equilibrium is estimated using the following equation[33]:

$$v_{CO_2,eq} = 4.137 \cdot 10^7 \ \exp\left(\frac{-20474}{T}\right) \quad (6)$$

Therefore, taking into account all the previous measurements and assumptions which affect the key variables in Eqs. 4 and 5, we can define the overall carbonator effectivity factor, φ_e, as:

$$\varphi_e = \frac{E_{carb} F_{CO_2}}{W_{CaO}/PM_{CaO}\ k_{reac-max} X_{active} (\overline{v_{CO_2}} - v_{CO_2,eq})_{reactor}} \quad (7)$$

The effectivity factor (φ_e) embraces all the physical resistances to the CO_2 carbonation process. φ_e should be equal to one when stationary state is achieved and then the

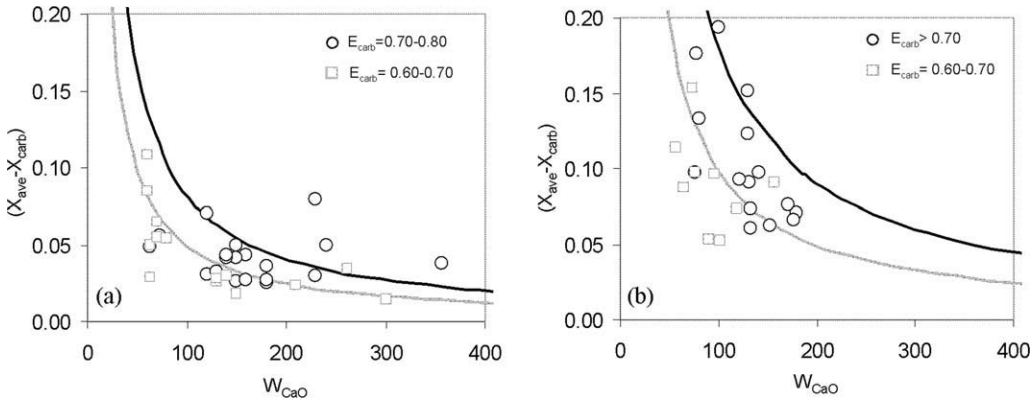

Figure 7. Active fraction of CaO as a function of the total solids bed inventory in the carbonator.

Average values of tendency lines. Graph (a) $u = 2$ m s^{-1}, $\varphi_s = 1.0$. Black line: $E_{carb} = 0.75$, $T_{carb} = 654$°C, $v_{CO_2} = 0.10$; Gray line: $E_{carb} = 0.65$, $T_{carb} = 647$°C, $v_{CO_2} = 0.12$. Graph (b) $u = 3$ m s^{-1}, $\varphi_s = 1.0$. Black line: $E_{carb} = 0.75$, $T_{carb} = 672$°C, $v_{CO_2} = 0.21$. Gray line: $E_{carb} = 0.65$, $T_{carb} = 668$°C, $v_{CO_2} = 0.17$.

overall kinetic reaction rate of the active part of the CaO is the controlling step of the CO_2 capture process in the carbonator reactor. All the terms on the right-hand side of this equation can be estimated experimentally for each stationary state period defined by the average temperature in the carbonator, the average gas velocity, and the average CO_2 concentration at the entrance to the carbonator reactor. The gas composition at the exit of the carbonator reactor is obtained from the gas analyzers. Therefore, the amount of CO_2 that disappears from the gas phase can also be calculated. The denominator of Eq. 7 is estimated by analyzing the solids samples obtained from each experiment to determine their carbonation conversion and their maximum carbonation conversion at the end of the fast reaction period (and hence X_{active}). The average CO_2 concentration can also be estimated as the mean logarithmic average of the values measured at the entrance and at the exit of the reactor.

Figure 5 compares the experimental values of the numerator and denominator of Eq. 7 as CO_2 flows through the cross-sectional area of the riser. The best fit for the slope obtained in this comparison yields a carbonator effectivity factor of 0.87. This value means that solids in the carbonator are 87% as effective for capturing CO_2 as those reacting in a differential carbonator reactor at the same average CO_2 concentration. Such a high-carbonator effectivity factor indicates that the overall carbonation reaction process in the carbonator reactor is mainly controlled by the relatively modest carbonation reaction rate of the bed material.

The previous discussion on the overall effectivity factor, and its role in reactor performance, paves the way for a more detailed discussion about the effects of the operating conditions and key variables on CO_2 capture efficiency.

Effect of the bed inventory of active CaO

Equations 4 and 5 establish a link between capture efficiency and the solids bed inventory of active material ($W_{CaO} \cdot X_{active}$) To illustrate this link using experimental results, the graphs in Figure 6 represent the variation in capture efficiency as a function of the amount of active CaO in the bed (kg m^{-2}). The solid lines in the graphs of the figure indicate the theoretical trend obtained from Eqs. 4 and 5. It can be observed from the tendency lines that the higher is the amount of active CaO inventory in the carbonator, the greater is the CO_2 capture efficiency. The dotted lines in Figure 6 indicate the average capture efficiency limit imposed by equilibrium under the average operational conditions of the experiments.

In the graphs of Figure 6, we have plotted examples of data sets under very stable operating conditions (specified in the legend). As can be seen, the agreement between the expected tendency line and the experimental data is very good for graphs (a–d) with an effectivity factor very close to 1. The graphs (e) and (f) show also good agreement with lower effectivity factors [0.6 for graph (e) and 0.5 for graph (f)]. The fitting of these points to Eq. 7 yields individual effectivity factors well below 1. This indicates lower gas–solids contact in the carbonator reactor and/or additional overall diffusion resistances to the reaction probably due to the higher reactivity of the material.

Figure 6 shows that a sufficient amount of active CaO is required in the carbonator reactor to achieve high-CO_2 capture efficiencies. The necessary amount of active CaO can be achieved by increasing the carrying capacity of the sorbent (and this is the aim of many fundamental research works recently published in the literature[4]). However, we simply note here that the same objective can be achieved by increasing the bed inventory. In practice, this variable is limited by fluid-dynamic restraints, but it is important for future research on this topic not to exaggerate the need for highly active materials, when this is only one of the terms affecting the overall reactor performance as defined in Eqs. 4 and 5.

Effect of the total CaO inventory

Figure 7 shows the changes in capture efficiency (E_{carb}) as a function of the total solids inventory (W_{CaO}) for a certain active fraction of CaO, ($X_{active} = X_{ave} - X_{carb}$). The solid lines in the graphs represent capture efficiency as a function of the solids inventory for the average value of the parameters involved in Eqs. 4 and 5 corresponding to the experimental dots plotted in each graph. The shaded areas between the lines

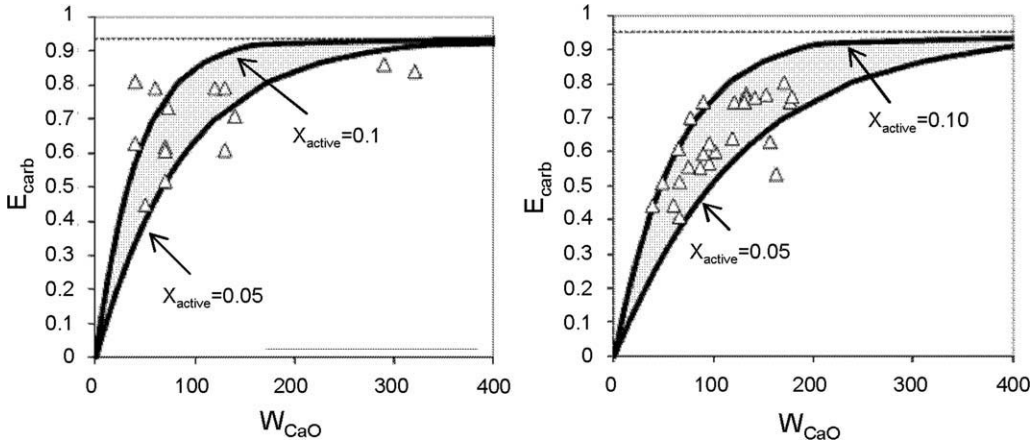

Figure 8. Capture efficiency as a function of the total CaO inventory in the carbonator.

Average values of tendency lines. Left graph: $T_{carb} = 636°$, $u = 2$ m s^{-1}, $v_{CO_2} = 0.11$, $\varphi_e = 1.0$; Right graph: $T_{carb} = 654°$C, $u = 3$ m s^{-1}, $v_{CO_2} = 0.18$, $\varphi_e = 1.0$.

represent the capture efficiency that can be achieved over the range of active fractions indicated in the graphs. The graph in the left side includes data obtained from experiments carried out at 2 m s^{-1}. The data set of the graph in the right was obtained from experiments carried out at 3 m s^{-1}. All the data in Figure 7 have an active fraction (X_{active}) between 0.05 and 0.1. As can be seen from the shaded areas, when the active fraction of CaO is high ($X_{active} > 0.05$), it is not necessary to operate with a high inventory of solids in order to achieve the maximum capture efficiency allowed by equilibrium. When the active fraction is below 0.05, increasingly larger inventories of solids are required to achieve high-capture efficiencies. The lines in the graphs in Figure 7 have been plotted assuming a carbonator effectivity factor of 1. There is reasonable agreement between most of the experimental points represented in the figure and the model, marked by the shaded area.

Figure 8 represents the combined effect of the solids inventory and solids carrying capacity on capture efficiency in the carbonator. The plots correspond to experimental data obtained from experiments carried out at 2 m s^{-1} [graph (a)] and 3 m s^{-1} [graph (b)], in which capture efficiencies are between 60 and 70% (gray dots) and higher than 70% (black dots). The solid lines represent the amount of active fraction of sorbent necessary for a given solids inventory in the bed to reach a capture efficiency of 65% (gray line) or 75% (black line). As can be seen in Figure 9, it is possible to achieve high-capture efficiencies with low-solids inventories (W_{CaO}), as long as there is a sufficient fraction of active calcium oxide (X_{active}) present in the bed to keep the product of both parameters constant. Alternatively, high-capture efficiencies are achieved using a high amount of solids (high W_{CaO}) of low-carrying capacity (low X_{active}).

Effect of the carrying capacity of the solids circulation flow

The characteristics of the solids inventory in the reactor, as discussed in previous sections, are determined by the carrying capacity of the solids circulation flow from the calciner ($F_{CaO} \cdot X_{ave}$) and its ratio to the total flow of CO_2 entering the reactor (F_{CO_2}). To obtain high-capture efficiencies, it is necessary that the circulating solids contain a sufficient amount of active CaO to capture all the CO_2 entering the carbonator ($F_{CaO} \cdot X_{ave}/F_{CO_2} > 1$).

In Figure 9, capture efficiency has been represented as a function of the variable $F_{CaO}X_{ave}/F_{CO_2}$. This parameter indicates the molar ratio of the active calcium oxide flow to the flow of CO_2 entering the reactor.

In Figure 9, for ratios of $F_{CaO}X_{ave}/F_{CO_2}$ lower than 1, the maximum capture efficiency is indicated by the black solid line. It can be seen that most of the experimental data with a ratio of $F_{CaO}X_{ave}/F_{CO_2}$ equal to or lower than 1 are close to the black line. In these cases, the limiting factor for capturing CO_2 is the low flow of active CaO in the circulating solids stream, due to the low-solid circulation rate, low-X_{ave} or low-calcination reaction efficiency (high X_{calc}).

If the ratio $F_{CaO}X_{ave}/CO_2$ is larger than one, the maximum capture efficiency is determined by the limitations of the equilibrium (dashed line in the figure, calculated for the average

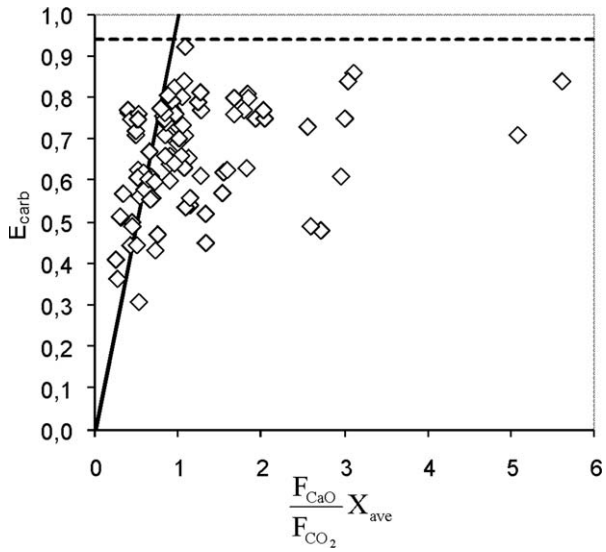

Figure 9. Variations of CO_2 capture efficiency vs. the carrying capacity of the solids circulating between the calciner and carbonator.

operational conditions of the entire set of experimental data). All the dots with a ratio of $F_{CaO}X_{ave}/CO_2$ larger than one should reach capture efficiency close to that allowed by the equilibrium. The dots in the figure with $F_{CaO}X_{ave}/CO_2$ ratios much larger than one and which do not reach maximum capture efficiency correspond to points where there is insufficient contact time between the solid phase and the gas phase in the reactor (because of low-solid inventory or low-carrying capacity, as discussed in the previous sections).

Conclusions

The CFB carbonator reactor required to operate a postcombustion CO_2 capture process based on calcium looping has been shown to yield high-capture efficiencies in a wide range of experimental conditions. Experiments in a test facility designed to test the carbonator reactor in conditions close to those expected for commercial applications have consistently yielded CO_2 capture efficiencies of between 70% and 90% with modest bed inventories (below 400 kg m^{-2}) and measured solids circulation rates of between 0.5 and 2.2 kg m^{-2} s^{-1}. The closure of the carbon balances between the CO_2 that has been captured from the gas phase and the $CaCO_3$ circulating between carbonator and calciner was found to be satisfactory in many stationary conditions. If the experimental results are compared with predictions from a simple reaction model applied to the solids samples extracted from the bed, an effectivity factor of around 0.87 is derived. This indicates the reaction rates controlled by the slow carbonation reaction that is characteristic of solids highly cycled between carbonation and calcination conditions. The key parameter for interpreting the experimental trends of the CO_2 capture efficiency is the product of the bed inventory of CaO and the fraction of active CaO in the bed. Moreover, it is a necessary, though insufficient, condition that a recycled stream of solids with sufficiently active CaO enters the carbonator to react with the CO_2 flow entering the reactor. When this condition is fulfilled, it has been shown that the low-carrying capacity characteristic of highly cycled CaO particles can be counterbalanced by sufficiently large inventories of solids in the CFB carbonator, that by increasing the average residence time of particles in the reactor, can increase the carbonation conversion achieved by CaO to values close to the maximum carrying capacity of the material.

Acknowledgments

This work was possible thanks to a contract with the companies Endesa and Hunosa and to the CaOling project funded by the European Commission FP7. N. Rodríguez acknowledges a fellowship awarded by FICYT. The assistance of B. González, F. Fuentes, and I. Rodríguez during the experiments and sample analysis is also acknowledged.

Notation

$dX_{carb}/dt|_{reactor}$ = average reaction rate of the solids in the reactor in relation to the average temperature and CO_2 concentration in the carbonator (s^{-1})
E_{carb} = CO_2 capture efficiency
$E_{carb,\ eq}$ = maximum CO_2 capture efficiency limited by the equilibrium
X_{active} = fraction of active CaO reacting in the fast reaction regime
F_0 = make up flow of fresh limestone (mol m^{-2} s^{-1})
F_{CaO} = solids molar flow in the recycling stream (mol m^{-2} s^{-1})
F_{CO_2} = CO_2 molar flow entering the carbonator (mol m^{-2} s^{-1})
G_s = solids circulation rate (kg m^{-2} s^{-1})
$k_{reac\text{-}max}$ = constant reaction rate obtained from tests with limestone in the thermobalance (s^{-1})
PM_{CaO} = average molar weight of the solids inventory in the carbonator (kg mol^{-1})
T_{carb} = average temperature of the carbonator reactor (°C)
$T_{CB}1$, $T_{CB}2$, $T_{CB}3$ = temperature measurements by thermocouples installed in the carbonator of the facility (Figure 2)
$T_{CC}1$, $T_{CC}2$, $T_{CC}3$ = temperature measurements by thermocouples installed in the calciner of the facility (Figure 2)
u = superficial gas velocity (m s^{-1})
X_{ave} = maximum average carbonation conversion
X_{calc} = $CaCO_3$ fraction of solids coming from the calciner
X_{carb} = $CaCO_3$ fraction of solids leaving the carbonator
W_{CaO} = total inventory of solids in the carbonator (kg m^{-2})

Greek letters

ΔX = net carbonation conversion in the carbonator reactor
φ_e = effectivity factor
$\overline{v_{CO2}}$ = average volume fraction of CO_2 in the carbonator
$v_{CO_2,0}$ = volume fraction of CO_2 at the inlet of the carbonator
$v_{CO_2,eq}$ = equilibrium volume fraction of CO_2 in the carbonator

Literature Cited

1. Intergovernmental Panel on Climate Change (IPCC). Special report on carbon dioxide capture and storage. Cambridge University Press. 2005.
2. Shimizu T, Hirama T, Hosoda H, Kitano K, Inagaki M, Tejima K. A twin fluid-bed reactor for removal of CO_2 from combustion processes. *Trans Inst Chem Eng*. 1999;77:62–68.
3. Harrison DP. Sorption-enhanced hydrogen production: a review. *Ind Eng Chem Res*. 2008;47:6486–6501.
4. Anthony EJ. Solid looping cycles: a new technology for coal conversion. *Ind Eng Chem Res*. 2008;47:1747–1754.
5. Curran GP, Fink CE, Gorin E. CO_2 acceptor gasification process. Studies of acceptor properties. *Adv Chem Ser*. 1967;69:141–161.
6. Balasubramanian B, Ortiz AL, Kaytakoglu S, Harrison DP. *Hydrogen from methane in a single-step process*. In: *Proceedings of the 15th International Symposium on Chemical Reaction Engineering (ISCRE 15)*, Newport Beach, California, 1998.
7. Silaban A, Harrison DP. High temperature capture of carbon dioxide: characteristics of the reversible reaction between CaO(s) and CO_2(g). *Chem Eng Commun*. 1995;137:177–190.
8. Han C, Harrison DP. Simultaneous shift reaction and carbon dioxide separation for the direct production of hydrogen. *Chem Eng Sci*. 1994;49:5875–5883.
9. Abanades JC. The maximum capture efficiency of CO_2 using a carbonation/calcination cycle of CaO/$CaCO_3$. *Chem Eng J*. 2002;90: 303–306.
10. Gupta H, Fan LS. Carbonation-calcination cycle using high reactivity calcium oxide for carbon dioxide separation from flue gas. *Ind Eng Chem Res*. 2002;41:4035–4042.
11. Haines M. IEAGHG high temperature looping cycle network, Greenhouse issues no. 96. IEA Greenhouse Gas Program, January 2010. Available at: http://www.ieaghg.org.
12. Abanades JC, Anthony EJ, Wang JS, Oakey JE. Fluidized bed combustion systems integrating CO_2 capture with CaO. *Envrion Sci Technol*. 2005;39:2861–2866.
13. Rodriguez N, Alonso M, Grasa G, Abanades JC. Heat requirements in a calciner of $CaCO_3$ integrated in a CO_2 capture system using CaO. *Chem Eng J*. 2008;138:148–154.
14. Romeo LM, Abanades JC, Escosa JM, Paño J, Giménez A, Sánchez-Biezma A, Ballesteros JC. Oxyfuel carbonation/calcination cycle for low cost CO_2 capture in existing power plants. *Energy Convers Manage*. 2008;49:2809–2814.

15. Li Y, Nie L, Hu XK, Yue GX, Li WK, Wu YX, Lu JF, Che DF. *Structure and performance of a 600 MWe supercritical CFB boiler with water cooled panels*. In: *Proceedings of the 20th International Conference on Fluidized Bed Combustion*, 2009, Tsinghua University Press, Xi'an (China), 1, 132–136.
16. Koppatz S, Pfeifer C, Rauch R, Hofbauer H, Marquard-Moellenstedt T, Specht M. H-2 rich product gas by steam gasification of biomass with in situ CO_2 absorption in a dual fluidized bed system of 8 MW fuel input. *Fuel Process Technol*. 2009;90:914–921.
17. Abanades JC, Anthony EJ, Lu DY, Salvador C, Alvarez D. Capture of CO_2 from combustion gases in a fluidized bed of CaO. *AIChE J*. 2004;50:1614–1622.
18. Fennell PS, Pacciani R, Dennis JS, Davidson JF, Hayhurst AN. The effects of repeated cycles of calcination and carbonation on a variety of different limestones, as measured in a hot fluidized bed of sand. *Energy Fuels*. 2007;21:2072–2081.
19. Fang F, Li ZS, Cai NS. Experiment and modeling of CO_2 capture from flue gases at high temperature in a fluidized bed reactor with Ca-based sorbents. *Energy Fuels*. 2009;23:207–216.
20. Lu DY, Hughes RW, Anthony EJ. Ca-based sorbent looping combustion for CO_2 capture in pilot-scale dual fluidized beds. *Fuel Process Technol*. 2008;89:1386–1395.
21. Symonds RT, Lu DY, Hughes RW, Anthony EJ, Macchi A. CO_2 capture from simulated syngas via cyclic carbonation/calcination for a naturally occurring limestone: pilot-plant testing. *Ind Eng Chem Res*. 2009;48:8431–8440.
22. Charitos A, Hawthorne C, Bidwe AR, Holz H, Pfeifer T, Schulze A, Schlegel D, Schuster A, Scheffknecht G. *Parametric study on the CO_2 capture efficiency of the carbonate looping process in a 10 kW dual fluidized bed*. In: *Proceedings of the the 20th International Conference on Fluidized Bed Combustion*, 2009, Tsinghua University Press, Xi'an (China), 1, 583–589.
23. Alonso M, Rodríguez N, González B, Grasa G, Murillo R, Abanades JC. Carbon dioxide capture from combustion flue gases with a calcium oxide chemical loop. Experimental results and process development. *Int J Greenhouse Gas Control*. 2010;4:167–173.
24. González B, Grasa GS, Alonso M, Abanades JC. Modeling of the deactivation of CaO in a carbonate loop at high temperatures of calcination. *Ind Eng Chem Res*. 2008;47:9256–9262.
25. González B, Alonso M, Abanades JC. Sorbent attrition in a carbonation/calcination pilot plant for capturing CO_2 from flue gases. *Fuel*. 2010;89:2918–2924.
26. Grasa GS, Abanades JC, Alonso M, Gonzalez B. Reactivity of highly cycled particles of CaO in a carbonation/calcination loop. *Chem Eng J*. 2008;137:561–567.
27. Grasa GS, Alonso M, Abanades JC. Sulfation of CaO particles in a carbonation/calcination loop to capture CO_2. *Ind Eng Chem Res*. 2008;47:1630–1635.
28. Li Y, Buchi S, Grace JR, Lim CJ. SO_2 removal and CO_2 capture by limestone resulting from calcination/sulfation/carbonation cycles. *Energy Fuels*. 2005;19:1927–1934.
29. Sun P, Grace JR, Lim CJ, Anthony EJ. Removal of CO_2 by calcium-based sorbents in the presence of SO_2. *Energy Fuels*. 2007;21:163–170.
30. Bhatia SK, Perlmutter DD. Effect of the product layer on the kinetics of the CO_2-lime reaction. *AIChE J*. 1983;29:79–86.
31. Dennis JS, Hayhurst AN. The effect of CO_2 on the kinetics and extent of calcination of limestone and dolomite particles in fluidised beds. *Chem Eng Sci*. 1987;42:2361–2372.
32. Grasa G, Murillo R, Alonso M, Abanades JC. Application of the random pore model to the carbonation cyclic reaction. *AIChE J*. 2009;55:1246–1255.
33. Baker EH. The calcium oxide-calcium dioxide system in the pressure range 1–300 atmospheres. *J Chem Soc*. 1962;464–470.

Manuscript received Mar. 4, 2010, and revision received May 6, 2010.